

Mechanical properties of hollow glass waveguides

Christopher D. Rabii
James A. Harrington, MEMBER SPIE
Rutgers University
Ceramic and Materials Engineering
607 Taylor Road
Piscataway, New Jersey 08854-8065
E-mail: jaharrin@rci.rutgers.edu

Abstract. Hollow glass waveguides with losses as low as 0.2 dB/m at the 10.6 μm are an attractive fiber delivery system for a broad range of IR wavelengths. These guides are made by depositing, using liquid-phase chemistry methods, silver and silver iodide films on the inside of silica tubing. The wet-chemistry techniques used in the process reduce somewhat the mechanical properties of the hollow-silica guides compared to the uncoated tubing used to make the guides. In particular, the mean failure stress is reduced from 8.4 GPa for uncoated, as-drawn, 530- μm bore silica tubing to 6.12 GPa for the Ag/AgI coated, 530- μm bore waveguide. In addition, the Weibull modulus decreases from 96.9 to 17. This means that the bending radius of the hollow guides, which is inversely proportional to the mean failure stress, increases from about 1 to about 1.5 cm. The reason for the decrease in strength for the processed tubing is the slow reaction of the aqueous coating solutions with the silica surface. Nevertheless, the bending radii for the guides is still quite small and the fatigue behavior of the guides, as measured by the crack growth parameter n , is essentially the same for processed or uncoated tubing. © 1999 Society of Photo-Optical Instrumentation Engineers. [S0091-3286(99)02009-7]

Subject terms: fiber optics; fiber optic applications; infrared fibers; hollow waveguides; mechanical properties of fibers; fiber reliability.

Paper 980311 received Aug. 14, 1998; revised manuscript received Feb. 17, 1999; accepted for publication Apr. 15, 1999.

1 Introduction

Hollow-core waveguides have been studied for many years in an effort to produce an efficient waveguide for use in medical and industrial applications.¹ The hollow glass waveguides (HGWs) that we have developed at Rutgers have very low loss for hollow guides operating between 3 and 12 μm . Not only is the loss as low as 0.2 dB/m but the HGWs have broadband transmission, good output mode properties, and flexibility. Many of the optical properties of HGWs have been investigated previously,²⁻⁴ but there have been only limited studies of the flexibility and mechanical properties of the waveguides.

The leaky-type of hollow waveguide consists of a structural tube that has metallic and dielectric films deposited on its inner surface to provide high reflectivity. The substrate tubing can be plastic, metal, or glass. The other type of hollow guide is an attenuated total reflectance guide. In this structure, the refractive index of the inner wall material is less than 1 in the spectral region of interest, and, therefore, with an air core (index of 1) the light guiding mechanism is similar to that of solid-core fibers. Sapphire (single crystal Al_2O_3) at 10.6 μm is an example of a material that has been used successfully as an $n < 1$ waveguide.¹

An important characteristic for any fiber delivery system is the need for both robustness and flexibility. The flexibility of hollow waveguides and solid-core fibers is inversely proportional to the moment of inertia of the fiber and its elastic modulus. The moment of inertia for cylindrical fibers increases as the fiber radius to the fourth power, mak-

ing the flexibility very sensitive to the radial dimension of the fiber. The robustness or strength of the waveguide, however, is a more complex matter. The mechanical strength of fibers depends on many factors that have been well documented for traditional solid-core glass optical fibers, and many of the techniques and assumptions used in evaluating their mechanical properties can be applied to the investigation of HGWs and their mechanical properties.

2 Fiber Strength and Reliability

Glass and ceramic materials have unique failure mechanisms, and as a result, cannot simply be classified by using an intrinsic value for strength. This situation arises because of the brittle nature of these materials and their inability to forgive slight flaws, which result in catastrophic failure at high stresses. Metals and plastics are not as sensitive to flaws, primarily because of their ability to plastically deform when subjected to stress. Plastic deformation results in a gradual, energy-absorbing failure. These two types of mechanical behavior are illustrated in the generic stress-strain curves shown in Fig. 1. The influence of external and internal flaws on the strength of brittle materials necessitates an approach to evaluating reliability in a way that gauges both the average strength and the distribution of strength for a given sample population. A comprehensive investigation of the strength of optical waveguides will also include the time dependence of strength, because environmental moisture promotes strength degradation, or fatigue by stress corrosion cracking.⁵

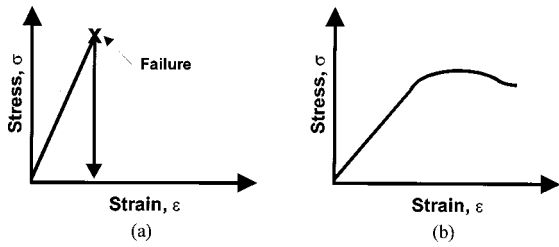


Fig. 1 Generic stress-strain behavior for (a) glasses or ceramics and (b) metals or plastics.

Experience with solid-core silica fibers has shown that flaws generated by improper manufacturing and handling practices will dramatically lower the strength of fibers.⁶ The inevitable presence of flaws with varying size, location, and orientation in a brittle material lends itself to a stochastic nature of quantifying strength. In general form, fiber failure can be viewed as a weakest-link model, where the cumulative probability for failure is given by⁷

$$F(\sigma^*) = 1 - \exp \left[- \int_A f(\sigma) dA \right], \quad (1)$$

where A represents the dimension of the sample. The quantity $f(\sigma)$ represents the probability per unit area that failure has occurred at the failure stress σ . Incorporated in this distribution is the dependence of failure probability on sample size and, as expected, the larger the sample, the higher the probability of encountering a flaw. The Weibull distribution is often used to describe the statistical nature of the flaws found in glass and ceramic materials based on the size and distribution of flaws. The cumulative probability of failure for the Weibull distribution is given by

$$f(\sigma) = 1 - \exp \left[\left(\frac{\sigma}{\sigma_0} \right)^m \right], \quad (2)$$

where σ is the failure stress; σ_0 is a normalizing constant; and m is the Weibull parameter, which is an inverse measure of the width of the strength distribution. The Weibull parameter for traditional telecommunications grade optical fiber can range from ~ 5 for weak fiber to > 100 for pristine silica.⁵

There are many methods used to measure the strength needed to obtain Weibull statistics. Techniques include simple tensile testing; mandrel bending, in which the fiber is wrapped around a cylinder of known radius; and two-point bending.⁵ Each test method relies on applying a known level of stress (or strain) to the fiber and recording when the fiber fails. Tensile testing applies stress uniformly over long lengths, but it can be costly and time consuming. Mandrel bending, where a fiber is wrapped around a cylinder of known size, is a very simple method, but the applied stress is fixed for each cylinder size. The method we used to determine the strength of the HGWs is two-point bending.⁸ The advantages of two-point bending are small gauge lengths, no fiber gripping as in tensile testing,⁹ and the ability to test multiple fiber samples at one time. In two-point bending, the fiber is loaded between two parallel, grooved faceplates and the stress is increased as the plates move together. This test method can also be used to analyze the static fatigue of the fiber through the measurement of time to failure at a constant faceplate separation. The apparatus used in two-point bending is schematically illustrated in Fig. 2. As the gap between the faceplates is reduced, the maximum strain ϵ_f experienced by the sample increases as

$$\epsilon_f = 1.198 \cdot \frac{d_{\text{glass}}}{D - d_{\text{total}}}, \quad (3)$$

where d_{glass} is the diameter of the glass fiber, d_{total} is the diameter of the coated fiber, and D is the distance between the faceplates at failure.⁸ The failure strain can then be related to the failure stress through Hooke's law:

$$\sigma = E(\epsilon)\epsilon_f, \quad (4)$$

where σ is stress and $E(\epsilon)$ is the elastic modulus. The elastic modulus is a function of strain because the high level of strains observed in strong fibers induces nonlinear changes in the elastic modulus. For this reason, the elastic modulus is often given by a polynomial approximation:

$$E(\epsilon) = E_0(1 + \alpha\epsilon + \beta\epsilon^2), \quad (5)$$

where E_0 is the elastic modulus at zero strain.⁹

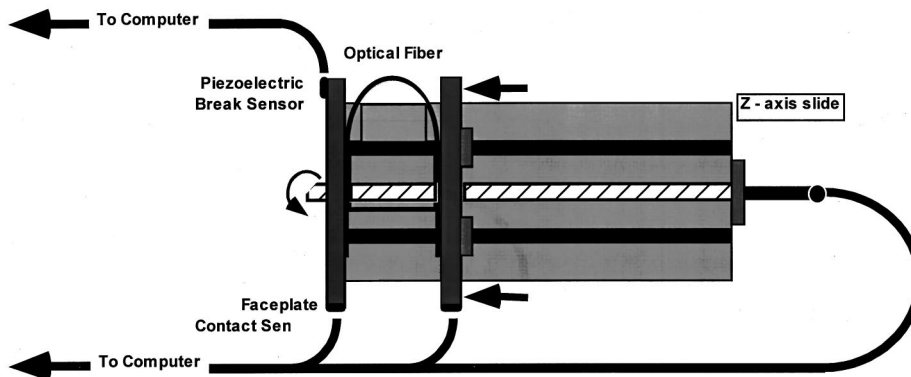


Fig. 2 Schematic of the two-point bend apparatus used for reliability testing of HGWs.

The most important disadvantage inherent in the two-point technique lies in the small length of fiber that is actually tested. The region of maximum stress in the sample lies midway between the faceplates, and the effective length under high stress depends on the strength of the sample itself.⁸ For this reason, two-point bending may not be an ideal test method for evaluating the mechanical behavior of long lengths of fiber. However, the length of HGW used in specialty applications is normally less than 10 m and, therefore, two-point bending is a good technique for our guides. To improve the statistics of the strength tests, it is necessary to test a large number of samples. In general, the mean failure stress that is predicted by two-point bend testing tends to overestimate the mean failure stress compared to testing a similar sample in tension. This effect is magnified for weak samples, and sample sets with low Weibull modulus.⁸

A complete analysis of the mechanical properties of an optical fiber includes the time dependence of strength. This is necessary because silica, and other materials, can experience a loss in strength when subjected to low levels of stress. In the case of silica, stress corrosion occurs in a moist environment. The reduction in stress occurs at low stress values because of the ability for atmospheric moisture working in conjunction with subcritical stresses to rupture the strained silicon-oxygen bonds forming the glass network.¹⁰ The level of subcritical stress is related to the stress intensity K_I and its critical value K_{IC} . The stress level K_I is given by

$$K_I = Y \sigma_a \sqrt{c}, \tag{6}$$

where σ_a is the applied stress, Y is a dimensionless parameter of order unity that depends on the crack shape, and c is the crack length. When stress at the crack tip produces a stress intensity factor below K_{IC} , the level of stress is designated as subcritical. If K_I exceeds K_{IC} , the crack propagates rapidly and failure occurs. This process of fatigue affects preexisting cracks in a material, essentially enlarging smaller flaws. The slow crack growth is generally assumed to follow a power-law dependence,

$$\frac{dc}{dt} = AK_I^n, \tag{7}$$

where the time dependence of crack length can be used to calculate the time to failure for a given applied stress level. This leads to the general expression,

$$t_f = B \frac{\sigma_i^{n-2}}{\sigma_a^n}, \tag{8}$$

where B is a constant representing several variables,¹¹ and is given by

$$B = \frac{2}{AY^2(n-2)K_{IC}^{n-2}}. \tag{9}$$

This expression is strongly dependent on the value of n and can be used to predict the lifetime of fiber under different

static stress conditions. The value of n is determined under dynamic fatigue conditions, where the failure stresses are recorded for different loading rates. Loading rates can be established under constant stress, strain, or faceplate velocity conditions. In particular, the relationship between failure stress and faceplate velocity is given by⁹

$$\sigma_f^{n-1} = \frac{(n-1)}{(n-2)} \frac{0.835}{rEAY^2} \left(\frac{\sigma_{IC}}{K_{IC}} \right)^{n-2} v. \tag{10}$$

Thus, the value of n can be obtained from the slope of a log-log plot of failure stress versus loading rate. Specifically, the slope is given by $(n-1)^{-1}$ for the constant faceplate velocity mode.

3 Experimental Methods

The two-point bending method was used to determine the strength parameters for all HGW samples. The mechanical reliability for guides at different stages of the fabrication process was determined from measurements of several different sample populations chosen to help elucidate the reasons for any process-induced weakening. In the first set of experiments, the silica guides had a 530- μm bore size with an outer glass diameter of 630 μm . Between 30 and 50 samples were fractured to obtain a high degree of confidence in the results. The temperature and relative humidity of each test have not been strictly controlled, but all tests were conducted within a temperature range of 18 to 21 $^{\circ}\text{C}$ and a relative humidity range of 20 to 30%.

The first sample population tested was the as-received, untreated tubing. This provided the baseline to compare to the treated tubing. The second sample set was again untreated tubing that had been flushed with clean house air. The third set was tubing that had been silver-coated using our standard mirror plating method.^{12,13} The samples in the fourth set were first sensitized using a SnCl_2 solution to enhance silver plating, then silvered in the same fashion as the third sample set. The fifth set consisted of samples of the finished waveguide with a metallic film of Ag followed by the deposition of a AgI film.¹⁴ The deposition of the dielectric layer involves flowing a solution of iodine in a nonaqueous solvent through the silvered tube.¹⁴ Finally, the last set of tubing was treated by using an aqueous solution consisting of distilled water with a pH of ~ 11.5 obtained by the addition of NH_4OH . This was done in an effort to duplicate the pH conditions of the silvering solution, without the deposition of any metal on the glass surface.

A second set of experiments was performed to evaluate the effect of glass-wall thickness on the strength distribution of unprocessed capillary tubing. The bore size of the waveguide is a critical parameter in determining the optical properties of the waveguide. It also has been shown that increasing the wall thickness in the waveguide can improve the modal properties of the waveguide.¹⁵ Increasing the outer dimension of the glass wall, however, will reduce the flexibility of the waveguide. Capillary tubing with i.d.:o.d. ratios of 700:800, 700:950, and 700:1100 μm was chosen for the tests. All tubing had an UV-acrylate coating on the outside surface for strength. In addition, different faceplate

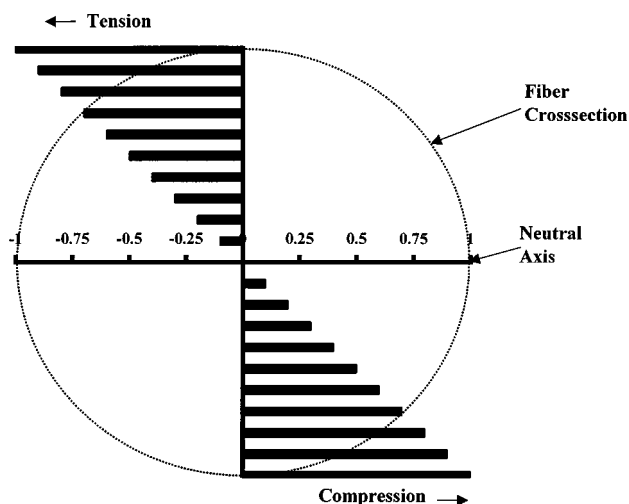


Fig. 3 Cross section of cylindrical fiber showing transition from tensile stress to compressive stress across neutral axis.

velocities of 100, 1000, and 10,000 $\mu\text{m}/\text{sec}$ were used for the determination of the fatigue parameter n for both processed and unprocessed samples.

4 Strength of Unprocessed Capillary Tubing

The most significant difference in terms of strength properties between solid-core optical fiber and HGWs is the presence of an inner surface. This inner surface manifests itself as an additional site for the possible initiation of critical flaws. The inner surface allows for surface damage, which might result during the draw or the thin-film coating stage of processing. If the flaws imparted during draw or processing become severe, the strength properties can be markedly degraded.

The stress distribution obtained in bend testing silica tubing can tell us about the magnitude of inner surface flaws and their impact on the strength of the capillary tubing. For an inner surface flaw to affect strength, it must be larger than similar outer surface flaws to be considered the failure-initiating or critical flaw. When an object of symmetrical cross section is subjected to a bending moment, a spectrum of stress states is induced in the material. Generally, the stress varies linearly from maximum tension on the outermost surface to maximum compression on the opposite surface of the fiber. A cross-sectional stress profile for a solid-core fiber is shown in Fig. 3. This figure illustrates the transition of stress from tension to compression when crossing the neutral or zero-stress axis of the fiber. This stress profile is approximated to first order using the relation⁸

$$\sigma = f(r) = \left(\frac{r}{R}\right)E, \quad (11)$$

where r is the distance from the neutral axis, and R is the radius of curvature of the fiber. This stress profile is applicable to hollow cylindrical shapes as well. The difference is that the neutral axis falls in a region where there is no material. For example, if the outer radius of the glass tubing is 315 μm and the inner radius is 265 μm , the stress on the

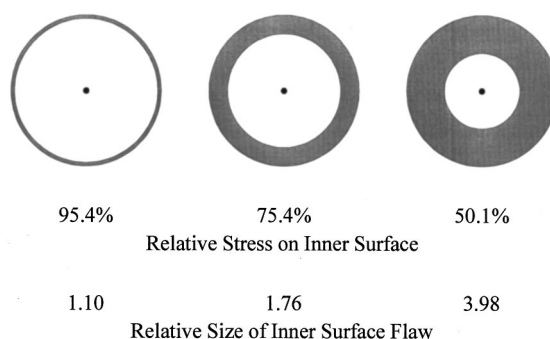


Fig. 4 Effect of wall thickness on stress at inner surface of tubing and reduction in flaw sensitivity.

inner surface would be approximately 84.1% of the maximum value at the outer surface, as predicted by Eq. (11). This means that for failure to occur at an inner surface flaw, it must be approximately 1.4 times as large as an outer surface flaw. In general, thick-walled tubing with the same bore size will be less sensitive to flaws on the inner surface than thin-walled tubing. The effect of wall size is illustrated schematically in Fig. 4. However, for low loss we want to have as large a bore as possible since the losses increase as $1/r^3$ and, thus, a thicker wall with a large bore means a larger bending radius.

The strength of silica fiber or capillary tubing that has been drawn and coated inline will have maximum strength immediately after fabrication. Subsequent handling and/or exposure to the atmosphere can only degrade the initial strength of the material. Therefore, we begin our evaluation of the mechanical properties by looking at our starting unprocessed capillary tubing fabrication. Figure 5 shows the strength data obtained for three different bore sizes of unprocessed tubing. The strength data for the 320- μm -bore tubing indicates that the tubing has a high median failure stress of 8.5 GPa but a fairly low Weibull modulus of 27.4. The median failure stress, or $\sigma_{50\%}$, is the level of stress at which the probability of failure (or survival) is 50%. For this waveguide, which has a i.d.:o.d.:coating ratio of 320:400:435 μm , this failure stress corresponds to a failure strain of 8.79%. Assuming that strain scales as r/R , as given by Eq. (7), the bend radius corresponding to this failure stress is calculated to be 0.45 cm. This is an extremely small bend radius when compared with other IR fibers, and it is adequate for even the tightest bends encountered in most applications. Similar data have been calculated for the other two bore-size fibers shown in Fig. 5, and these data are summarized in Table 1.

The data in Fig. 5 show the expected result that the effective bend radius at the 50% failure level increases as the outer diameter of the glass tubing is increased. The 530- μm -bore and the 700- μm -bore waveguides have almost identical outer diameters and, as a result, show similar 50% failure radii. It is important to remember that the 50% failure level is too high for most applications, as it does not provide a sufficient safety factor. In addition, the strength data obtained through the two-point bending technique only approximate the stress distribution encountered in real-life applications. This is because stress is distributed over a small region in two-point bending compared to the much

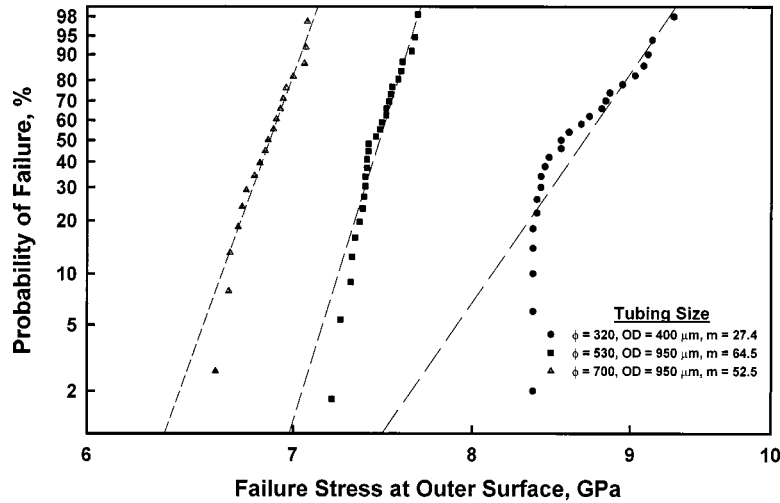


Fig. 5 Strength data and Weibull statistics generated for three bore sizes of uncoated capillary tubing used to make HGWs ($\nu = 1000 \mu\text{m/s}$).

larger region of maximum stress in pure tension. This difference can be reconciled using an approximation that adjusts the stress measured in two-point bending to that in tension derived by Matthewson et al.⁸

The Weibull modulus for the 320- μm -bore tubing is substantially lower than for the other two samples. This may be due to the fact that the outer coating of the 320- μm -bore tubing is polyimide rather than UV acrylate, which was used to coat the 530- and 700- μm -bore tubing. The UV acrylate coating is thicker than the polyimide coating and perhaps offers better protection from handling damage.

5 Effects of Processing on Strength

Processing the silica tubing to make HGWs involves the use of wet-chemistry methods, which can potentially degrade the strength of the inner surface. One of the first steps that we have used prior to applying the silver film is the removal of any dust or other particles from the inside of the capillary tubing using compressed dry air. The strength distributions of 530:630- μm -bore, unprocessed tubing compared to tubing cleaned with compressed air are shown in Fig. 6. We note that the untreated tubing (control sample group) has extremely high strength and a very narrow distribution. Its high Weibull modulus of $m = 96.9$ is comparable to that of high-quality telecommunications-grade

silica optical fiber. In addition, the 50% failure stress ($\sigma_{50\%}$) corresponds to a bend radius of approximately 0.35 cm.

The strength data for the tubing cleaned using compressed air are compared to the unprocessed tubing in Fig. 6. The majority of the air-cleaned samples showed strength values identical to that of the control group. There is, however, a weak tail in the strength distribution, consisting of seven samples that fractured at stress levels considerably lower than the majority population. Any distribution with a weak tail poses a serious limitation on the usefulness of any waveguide processed in this manner. That is, 90% of the tubing can sustain stress levels >6 GPa but the other 10% will fail at levels closer to 3 GPa. If the weak tail shown in Fig. 6 is censored or omitted from the numerical analysis, then we see that the Weibull modulus $m = 100$ is similar to the control tubing for which $m = 96.9$.

Fractography, or analysis of fracture surfaces, is a technique often used to gather information on the cause of fracture that cannot be garnered solely through the examination

Table 1 Summary of Weibull statistics shown in Fig. 5 ($\nu = 10^3 \mu\text{m/s}$).

Tubing Configuration (μ_m)						
Bore	Glass o.d.	Coating o.d.	$\sigma_{50\%}$ (GPa)	$\epsilon_{50\%}$ (%)	Bend Radius at Failure (cm)	Weibull Modulus
320	400	435	8.545	8.79	0.46	27.4
530	950	1100	7.423	7.88	1.21	61.5
700	950	1250	6.870	7.41	1.28	52.5

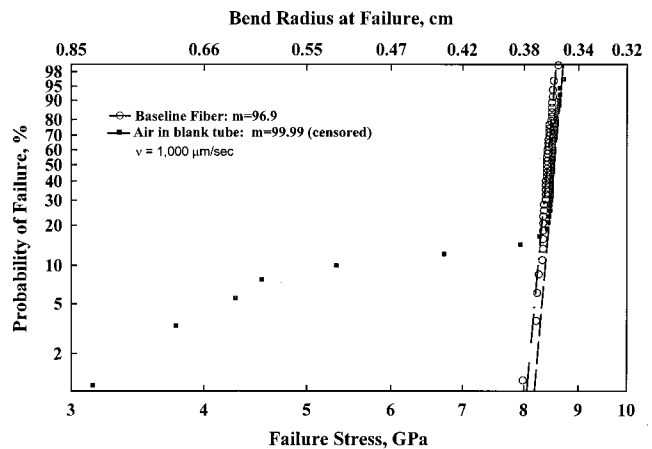


Fig. 6 Strength degradation resulting from compressed air cleaning of glass capillary tubing prior to coating.

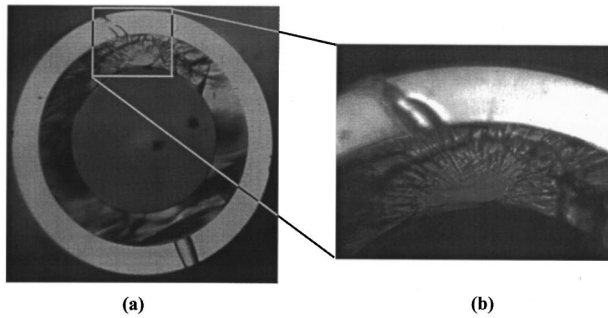


Fig. 7 Fracture surface (a) with enlarged region (b) showing possible inner surface flaw.

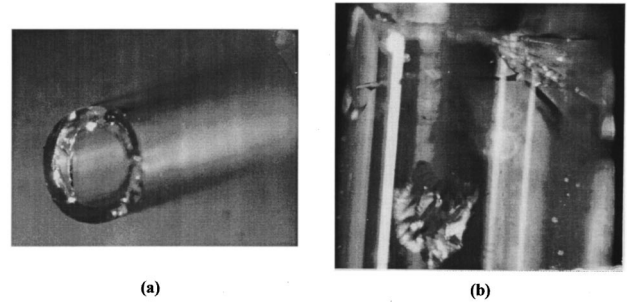


Fig. 8 End face (a) and side (b) of capillary tubing showing the presence of loose glass shards.

of numerical data.¹⁶ When the fracture surface shows a well-defined mirror, mist, and hackle region, fractography can be used to obtain the size of failure-initiating flaws.¹⁷ We have used fractography to study the low-stress failures observed in the airflow treated tubing. Figure 7 shows a micrograph of the cross section of a weak sample. The lighter cylindrical region in the micrograph is the UV acrylate coating, and the darker cylinder inside this is the wall of the glass tubing. A magnified region of the mirror region on the fracture surface of a weak sample is shown in Fig. 7(b). The details of this fracture surface indicate that the flaw leading to failure in this instance was located on the inner surface of the tubing. Further examination of similar weak tubing samples has revealed glass shards on the inner surface of the freshly cleaved capillary tubing as shown in Fig. 8. These glass shards, which occur as a result of cleaving the tubing, can be carried into the tubing weakening the inner surface. The proposed flaw initiation process is illustrated in Fig. 9. The compressed air flowing down the bore of the waveguide carries loose glass shards through the tubing where they contact the inner surface and initiate flaws. We eliminated flaws caused by shards by more careful scribing and discontinuing the use of the compressed air cleaning step without deleteriously affecting the quality of the deposited films.

The primary mechanism that degrades the strength of the tubing is the wet-chemistry processing used to apply the metallic and dielectric coatings to the inner surface of the tubing. To determine the extent of process-induced weak-

ening, we measured the strength of waveguides after each step in the waveguide fabrication process. For these measurements, the substrate tubing used was the same high-strength 530:630:950 μm tubing analyzed in the previous section. Again, the temperature and relative humidity for each test were within a temperature range of 18 to 21°C and a relative humidity range of 20 to 30%.

The strength distributions for sample sets 3 and 4 are given in Fig. 10 along with the control sample set 1. The silver-coated tubing samples (set 3) have a high mean-failure stress level of 6.99 GPa, but they are 17% weaker than the untreated sample set. More importantly, the strength distribution of the silvered tubing is wider than that of the control set, as evidenced by the decrease in the Weibull modulus from 96.9 to 22.7. The strength values for tubing that had been both sensitized and silvered (sample set 4) reveals that this processing reduces the strength even further. Specifically, the mean strength has decreased compared to the control sample by nearly 28% to 6.09 GPa and a Weibull modulus of 17.0.

The weakening of the HGWs is due to the interaction of the aqueous processing solutions with the silica. The silvering process involves the use of the base NH_4OH to raise the pH for optimum plating conditions. As a result, the final silvering solution has a pH of approximately 11.5. Silica surfaces are known to be susceptible to attack and dissolution by any pH solution, but the greatest effect is observed in basic solutions. The mechanism by which water corrodes

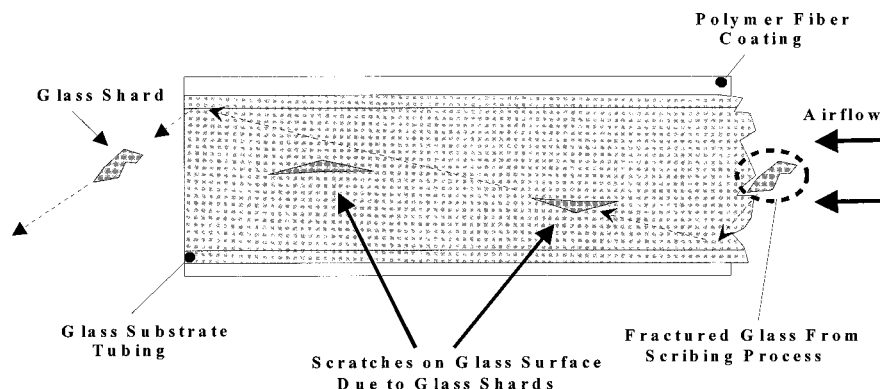


Fig. 9 Illustration of flaw initiation process due to presence of shards and airflow over uncoated glass surface.

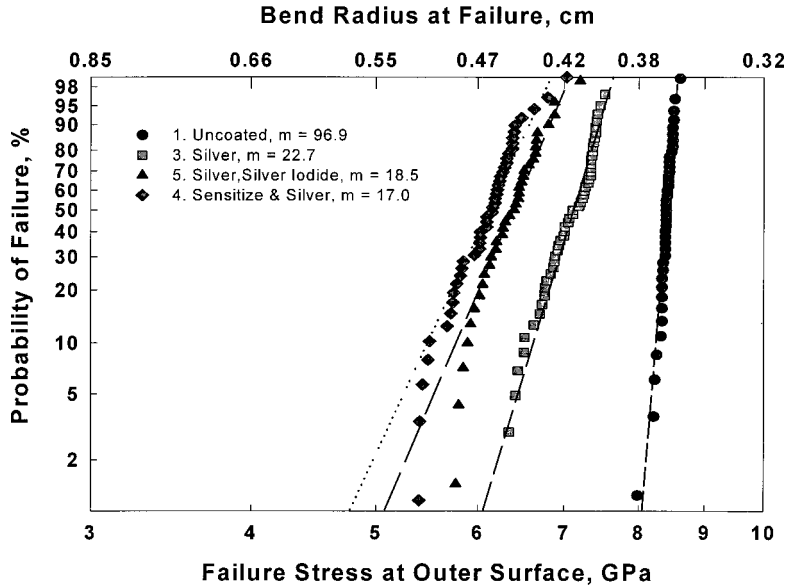
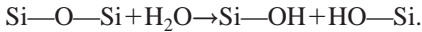


Fig. 10 Weibull statistics for the strength of waveguides after each processing stage: constant face-plate speed, $v = 1000 \mu\text{m/s}$; $T \sim 20^\circ\text{C}$, and relative humidity $\sim 25\%$. Note that failures occurring as a result of inner surface flaws imply tensile failure at lower stress levels, reduced by the ratio of i.d.:o.d., in this case $\sim 16\%$.

silica surfaces involves the approach of H_2O to a strained Si—O—Si site,¹⁰ allowing the reaction



The formation of silanol (Si—OH) units, depicted schematically in Fig. 11, permits small cracks to propagate and weaken the glass. The pH-dependent strength degradation of silica fiber has been observed¹⁸ and found to be most severe for basic solutions. Corrosion of silica is not limited to the aqueous species, and it has been shown that hydra-

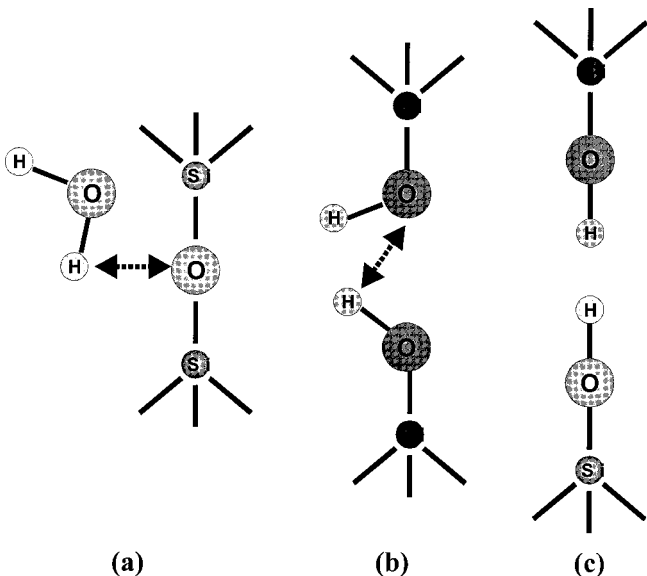


Fig. 11 Schematic of surface corrosion in silica glass: (a) adsorption, (b) reaction, and (c) hydroxyl formation.

zine (N_2H_4), formaldehyde (CH_3NO), and ammonia (NH_3) all possess the polar electron configuration that enables the same type of stress-activated corrosion observed with water.¹⁰ Therefore, the solutions that we use to adjust the pH are especially corrosive to silica surfaces because of the presence of both OH^- and NH_4^+ species.

We took fractographs of some of the processed waveguides that failed at low stress levels. A fracture surface from a silvered waveguide sample is shown in Fig. 12. The micrograph was obtained using a scanning electron microscope (SEM), and the image magnification is $800\times$. The dark area at the top, left-hand section of the micrograph is the bore of the tubing. The characteristic mirror, mist, and hackle regions are centered on a point on the inner surface of the tubing. This type of fracture pattern indicates that the flaw leading to failure was located near this point on the inner surface.

Sensitization of glass surfaces is a common method to ensure good adhesion between the deposited metal and substrate. The most common sensitizing agent used in the sil-

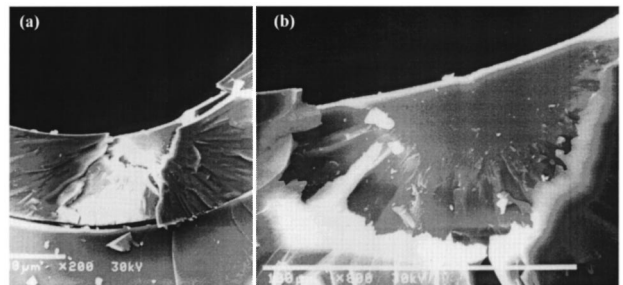


Fig. 12 SEM image of failure flaw on the inner surface of silvered capillary tubing, (a) $200\times$ magnification and (b) $800\times$ magnification.

vering process is a weak stannous chloride solution. Other metal salts, such as PdCl_2 and PtCl_2 also have similar effects on glass surfaces.¹⁹ In general, in this predeposition step, a thin layer of metal atoms is deposited on the surface of the glass, altering the glass surface to facilitate the deposition of the metal layer. Pretreatment sensitization is known to increase the density of island formation during the initial stages of aluminum plating.^{20,21} For Ag plating, molecular dynamics studies on the adsorption of thin metallic layers, similar to the sensitization process, on silica surfaces can significantly change the bond character of the surface.²² As a result, there can be a decrease in Si—O—Si bond angles on the silica surface. The decrease in bond angle acts to create an increased number of reactive sites that can lead to uniform plating and an improvement in silver adhesion. These reactive sites can also offer low-energy locations for water molecules as well²³ and, therefore, increase the rate of corrosion similar to that which we observe. Webb and Garofalini have suggested that this type of modification of the silica surface, in conjunction with an aqueous environment, can lead directly to weakening and fatigue of silica glass.²³ The increase in reactivity of the glass surface due to sensitization correlates well with the decrease in strength of the silvered waveguide (set 3) and to the strength of the sensitized and silvered waveguides (set 4).

Finally, the strength properties of the complete HGW with Ag/AgI coatings were measured (sample set 5). The complete waveguide was silvered using the same procedure that was used to make the silver-only (set 3) guides. A dielectric layer with a thickness suitable for 10.6- μm transmission was then formed on the silver surface. The Weibull data for the finished guide shows that this waveguide is slightly weaker than the silver-only guide, but stronger than the sensitized and silvered guide (set 4).

The proposed weakening mechanism indicates that this type of weakening is likely to be observed in all HGWs processed using aqueous solution-based, liquid-phase deposition of silver films. It is possible that a different selection of solvents could be found that would not interact with the glass like the aqueous-based solvents but we have so far not found any such solvents. HGWs have also been fabricated using chemical vapor deposition²⁴ (CVD) techniques. In this gas-phase method, there are no aqueous solvents to come into contact with the bare silica surface. As a result, this fabrication method could offer some improvement in mechanical reliability, but the mechanical properties of these waveguides have not been studied.

6 Fatigue Behavior of Capillary Tubing

The lifetime and fatigue properties of the silica guides can be determined through a study of the time dependence of strength. One way to assess the susceptibility of a waveguide to fatigue is to measure the crack growth parameter n , defined in Eq. (6). Fatigue is important because waveguides are always subject to some stress, which can lead to deterioration of the strength in time and ultimately to fracture. The nature of the crack growth at subcritical stresses can be measured using one of several techniques. One method of measuring the stress-enhanced corrosion in silica fibers is through the application of a constant level of known stress and measuring the time to failure. This is

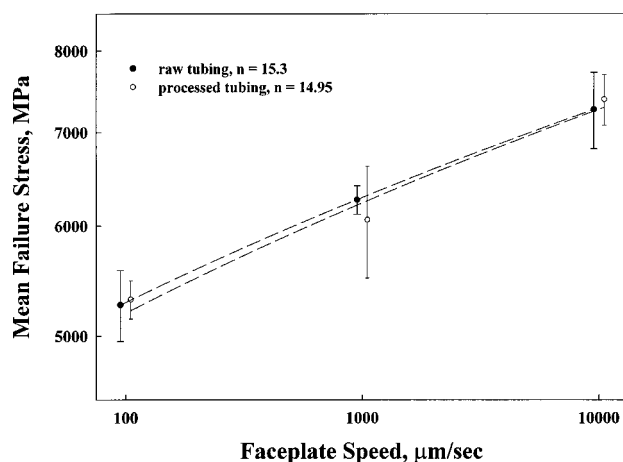


Fig. 13 Stress corrosion parameter, n , for unprocessed and processed 630 μm -bore tubing. The reasonably high value for n indicates that the reliability of the HGWs is close to that of conventional silica fiber optics. All tests were conducted at $T=20^\circ\text{C}$ and Rel. Hum.=25%.

static fatigue. Static fatigue is often an effective means of accurately reflecting the conditions encountered in many practical applications.⁵ One drawback is that low levels of applied stress result in long times to failure, making the experiment very time consuming. Another method involves measuring the fatigue of an optical fiber under dynamic stress conditions, greatly shortening the time for experimental analysis. The dynamic method makes use of the same two-point bending apparatus that we used to obtain the Weibull parameters. In addition, the dynamic fatigue applies for a variety of conditions, including constant faceplate velocity, constant strain rate, and constant stress rate.⁹ In our experiment, HGW samples are placed in the two-point bender and a constant face plate speed v is used. The value of n can be obtained by noting that the failure stress is simply related to the face plate speed, i.e.,

$$\sigma_f^{n-1} = \text{const } v. \quad (12)$$

When the average failure stress is plotted versus the logarithm of the loading rates, n may be determined from the slope, which is equal to $(n-1)^{-1}$.

Data were obtained for both raw tubing and fully processed waveguide samples. Faceplate velocities of 10^2 , 10^3 , and 10^4 $\mu\text{m}/\text{s}$ were used for each set of tubing. The UV acrylate coated tubing had an i.d.:o.d.:coating geometry of 630:845:1190 μm . The Weibull data indicate that all tested samples are extremely uniform with a high mean failure stress. The data are typical of fatigue data in that the samples fractured at the highest strain rates exhibit the highest average failure stress. To obtain a value for n , the average failure stress as a function of faceplate velocity for both the processed and unprocessed guides has been plotted on the log-log plot. Figure 13 shows that the values calculated for n for both uncoated and coated tubing are nearly identical, and they are in reasonable agreement with measurements previously obtained for strong UV acrylate coated fused silica optical fibers.⁹ From this we conclude that the unprocessed silica tubing and finished waveguides

Table 2 Summary of strength data obtained on processed waveguides.

Tubing Treatment	50% Failure Stress (GPa)	Mean Failure Stress (GPa)	Weibull Modulus (m)	95% Interval for m
1. Control	8.41	8.40±0.02	96.9	75.5–123.7
2. Airflow censored	8.54	8.53±0.01	99.9	77.0–128.8
3. Silver	7.06	6.99±0.07	22.7	18.4–27.8
4. Sensitize and silver	6.12	6.09±0.05	17.0	13.4–21.5
5. Silver and dielectric	6.39	6.36±0.06	18.5	14.1–24.1

Faceplate speed: 1000 $\mu\text{m/s}$, $T \sim 20^\circ\text{C}$, relative humidity $\sim 25\%$.

Table 3 Comparison of elastic properties of three major glass families.

Glass Family	Microhardness (GPa)	K_{IC} (MPa $m^{0.5}$)	Young's Modulus (GPa)	Shear Modulus (GPa)	Poisson's Ratio
Silica	7.7	0.75	73.1	31.2	0.17
Fluoride	2.2	0.3	51	20	0.3
Chalcogenide	1	0.25	20	7.5	0.26

will exhibit fatigue behavior similar to traditional solid-core silica fibers despite differences in geometry.

7 Conclusions

The strength of unprocessed silica tubing has been shown to approach the strength of conventional silica fibers used in telecommunication applications. However, when the tubing is processed using wet-chemistry methods the strength degrades as a result of the interaction between the aqueous solutions used in producing the silver and dielectric coatings and the silica wall. The Weibull modulus was seen to decrease from approximately 100 to less than 20 after processing. The strength results for all stages of the process from the unprocessed to the final completely coated waveguide are summarized in Table 2. Even though the tubing is somewhat weakened as a result of processing, the HGWs remain quite strong with bending radii less than 2 cm for the 530- μm -bore tubing. In practice, the adverse effects of processing on HGW reliability can be dealt with by proof testing⁵ the tubing after coating to ensure that the HGW has uniformly high strength. Subjecting the waveguides to a low level of stress after processing can isolate the weak portions of fiber and, therefore, increase the uniformity of the HGW. Silica tubing remains much stronger than IR glass fibers, as can be seen in a comparison of the elastic properties of silica, fluoride, and chalcogenide glass in Table 3. From this comparison, we see that the elastic properties of silica are better than both the fluoride and chalcogenide glass. Specifically, silica waveguides have better flexibility and higher strain to failure than any other IR waveguides.^{25–27} This fact combined with the very smooth surface of silica, the nontoxic nature of SiO_2 , and the low cost of silica waveguides provide an almost ideal structure for a hollow waveguide.

References

- J. A. Harrington and Y. Matsuura, "Review of hollow waveguide technology," *Proc. SPIE* **2396**, 4–14 (1995).
- J. A. Harrington, Ed., *Selected Papers on Infrared Fiber Optics*, SPIE Milestone Series, Vol. MS09, pp. 409–470, 527–537, SPIE, Bellingham, WA (1990).
- Y. Matsuura and M. Miyagi, "Bending losses and beam profiles of zinc selenide-coated silver waveguides for CO_2 laser light," *Appl. Opt.* **31**, 6441–6445 (1992).
- Y. Matsuura, T. C. Abel, J. Hirsch, and J. A. Harrington, "Small-bore hollow waveguide for delivery of near singlemode IR laser radiation," *Electron. Lett.* **30**, 1699–1689 (1994).
- M. J. Matthewson "Optical fiber mechanical testing techniques," in *Fiber Optics Reliability and Testing*, *Proc. SPIE* **CR50**, 32–59 (1994).
- C. R. Kurkjian, J. T. Krause, and M. J. Matthewson, "Strength and fatigue of optical fibers," *J. Lightwave Technol.* **7**, 1360–1370 (1989).
- W. Weibull, "The phenomenon of rupture in solids," *Proc. R. Swed. Inst. Eng. Res.* **153**, 3–55 (1939).
- M. J. Matthewson, C. R. Kurkjian, and S. T. Gulati, "Strength measurement of optical fibers by bending," *J. Am. Ceram. Soc.* **69**, 815–821 (1986).
- V. V. Rondinella and M. J. Matthewson, "Effect of loading mode and coating on dynamic fatigue of optical fiber in two-point bending," *J. Am. Ceram. Soc.* **76**, 139–144 (1993).
- T. A. Michalske and S. W. Freiman, "A molecular mechanism for stress corrosion in vitreous silica," *J. Am. Ceram. Soc.* **66**, 284–288 (1983).
- M. J. Matthewson, "Optical fiber reliability models," in *Fiber Optics Reliability and Testing*, *Proc. SPIE* **CR50**, 3–31 (1994).
- T. Abel, J. Hirsch, and J. A. Harrington, "Hollow glass waveguides for broadband infrared transmission," *Opt. Lett.* **19**, 1034–1036 (1994).
- N. Croitoru, J. Dror, and I. Gannot, "Characterization of hollow fibers for the transmission of infrared radiation," *Appl. Opt.* **29**, 1805–1809 (1990).
- K. Matsuura, Y. Matsuura, and J. A. Harrington, "Evaluation of gold, silver, and dielectric-coated hollow glass waveguides," *Opt. Eng.* **35**, 3418–3421 (1996).
- Y. Matsuura, C. D. Rabii, K. Matsuura, and J. A. Harrington, "Low order multimode generation in hollow glass waveguides," *Electron. Lett.* **32**, 1096–1098 (1996).
- T. A. Michalske, "Quantitative fracture surface analysis," in *Engineered Materials Handbook—Ceramics and Glasses*, Vol. 4, pp. 652–662, ASM International (1991).
- J. J. Mecholsky, R. W. Rice, and S. W. Freiman, "Prediction of fracture energy and flaw size in glasses from measurements of mirror size," *J. Am. Ceram. Soc.* **57**, 440–443 (1974).
- N. German and S. Yannacopoulos, "Environmental effects on the mechanical integrity of optical fibers," *Opt. Eng.* **36**, 1438–1442 (1997).
- B. Schweg, *Mirrors: A Guide to the Manufacture of Mirrors and Reflecting Surfaces*, Pelham, London (1973).
- K. Sugai, H. Okabayashi, T. Shinzawa, S. Kishida, A. Kobayashi, T. Yako, and H. Kadokura, "Aluminium chemical vapor deposition with new gas phase pretreatment using tetrakisdimethylamino-titanium for ultralarge-scale integrated-circuit metallization," *J. Vac. Sci. Technol. B* **13**, 2115–2118 (1996).
- K. Sugai, H. Okabayashi, S. Kishida, and T. Shinzawa, "Titanium-containing hydrofluoric acid pretreatment for aluminum chemical va-

- por deposition," *Thin Solid Films* **280**, 142–146 (1996).
22. D. C. Athanasopoulos and S. H. Garofalini, "Molecular dynamics simulations of the effect of adsorption on SiO₂ surfaces," *J. Chem. Phys.* **97**, 3775–3780 (1992).
 23. E. B. Webb III and S. H. Garofalini, "Molecular dynamics simulation of the approach and withdrawal of a model crystalline metal to a silica glass surface," *J. Chem. Phys.* **101**, 10101–10106 (1994).
 24. Y. Matsuura and J. A. Harrington, "Hollow glass waveguides with three-layer dielectric coating fabricated by chemical vapor deposition," *J. Opt. Soc. Am. A* **14**, 1255–1259 (1997).
 25. E. M. Dianov, V. M. Krasteva, V. G. Plotnichenko, S. L. Semenov, M. F. Churbanov, and I. V. Scripachev, "Mechanical properties of chalcogenide glass optical fibers," in *SPIE Infrared Fiber Optics II, Proc. SPIE* **1228**, 92–100 (1990).
 26. J. Colaizzi, M. J. Matthewson, T. Iqbal, and M. R. Shahriari, "Mechanical properties of aluminum fluoride glass fibers," in *Infrared Fiber Optics II, Proc. SPIE* **1591**, 26–33 (1991).
 27. N. Barkay and A. Katzir, "Mechanical resistance of silver halide infrared fibers," in *Infrared Fiber Optics III, Proc. SPIE* **1592**, 50–59 (1991).



Dr. Rabii is has been a member of SPIE since 1995.

Christopher D. Rabii graduated from Rutgers University, New Brunswick, New Jersey, in 1993. He received the MS and PhD degrees in ceramic and materials engineering from the same university in 1995 and 1998 respectively. In 1998 he joined Premier Laser Systems where he performs research and development work on fiber delivery systems for medical devices. His research interests include optical materials, hollow waveguides and specialty optical fibers.



for use as chemical and thermal fiber sensors. Specifically, these fibers include hollow glass waveguides and single-crystal sapphire fibers.

James A. Harrington is professor of ceramic and materials engineering at Rutgers University. Dr. Harrington's basic research interests are in the area of specialty fiber optics and the optical properties of solids. Since 1977, he has worked on all aspects of infrared fibers including fabrication, characterization, and applications. His current research interests include the development of IR fiber optics for use in the delivery of laser power in surgical and industrial applications and for use as chemical and thermal fiber sensors. Specifically, these fibers include hollow glass waveguides and single-crystal sapphire fibers.